ACS OMEGA

http://pubs.acs.org/journal/acsodf

Article

Effective Absorption Mechanism of SO_2 and NO_2 in the Flue Gas by Ammonium-Bromide-Based Deep Eutectic Solvents

Tengteng Zhou,[‖ T.Z. and Y.Z. c] Yongqi Zhao,[‖ T.Z. and Y.Z. c] Xinxin Xiao, Yixuan Liu, Hongcun Bai, Xingxing Chen, Jinxiao Dou,* and Jianglong Yu*

Cite This: *ACS Omega* 2022, 7, 29171−29180

Read Online

ACCESS | Metrics & More | Article Recommendations | Supporting Information

ABSTRACT: Simultaneous capture of SO_2 and NO_x from flue gas is critical for coal-fired power generation. In this study, environmentally friendly and high-performance deep eutectic solvents based on ethylene glycol and ammonium bromide were designed to capture SO_2 and NO_2 simultaneously. The SO_2 and NO_2 absorption performances and absorption mechanisms were systematically investigated by ^{1}H NMR and Fourier transform infrared (FT-IR) spectroscopy in combination with ab initio calculations using Gaussian software. The results showed that EG-TBAB DESs can absorb low concentrations of SO_2 and NO_2 from the flue gas simultaneously at low temperatures (≤50 °C). ^{1}H NMR, FT-IR, and simulation results indicate that SO_2 and NO_2 are absorbed by forming EG-TBAB-SO_2−NO_2 complexes, Br^- is the main active site for NO_2 absorption, and NO_2 is more active in an EG-TBAB-NO_2−SO_2 complex than SO_2. EG-TBAB DESs exhibit outstanding regeneration capability, and absorption capacities remain unchanged after five absorption−desorption cycles. The fundamental understanding of simultaneous capture of SO_2 and NO_2 from this study enables DES structures to be rationally designed for efficient and low-cost desulfurization and denitrification reagents.

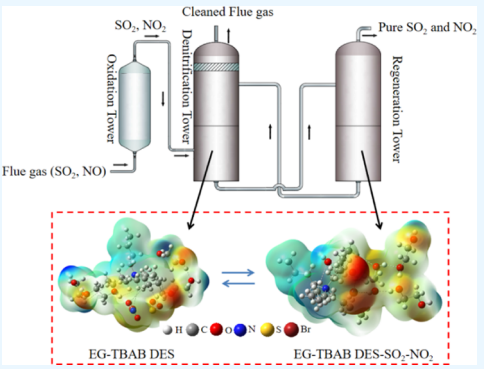

1. INTRODUCTION

Coal-burning releases large amounts of sulfur- and nitrogen-containing harmful emissions (SO_2 and NO_x), and these pollutants are the major causes of large-scale haze in China. To address the growing environmental dilemma, these harmful emissions should be removed from flue gas before being released into the atmosphere. At present, conventional flue gas treatment technology mainly revolves around flue gas desulfurization and denitrification treatment processes, performing wet desulfurization, selective catalytic reduction (SCR), and selective noncatalytic reduction (SNCR) denitrification. Although these techniques have a wide range of applications in the industry, they suffer shortcomings of high investment cost, complex process operation, generation of wastes, ammonia leakage, etc.[1−4]

In recent years, new innovative techniques for flue gas desulfurization and denitrification have been widely developed. Using ionic liquids (ILs) for the removal of SO_2 and NO_x in flue gas is one of the newly developed desulfurization and denitrification techniques.[3−7] An ionic liquid is a substance that is entirely composed of an anion and a cation and is liquid at normal temperature or near-normal temperatures. ILs possess many physicochemical properties including negligible vapor pressure,[8] high thermal stability,[9] low flammability,[10] capability to absorb most gases (such as SO_2, H_2S, CO_2, and other acid gases), and recyclability.[11] However, many literature works have also pointed out the high toxicity,[12] poor biodegradability,[13] combustible characteristic,[14] high viscosity,[15] or high-cost production of ILs,[16] which hinder their industrial applications. Instead of finding suitable candidates to replace ILs, researchers are developing new ways to exploit the positive properties of ILs while avoiding their negative characteristics. Deep eutectic solvents (DESs) have been introduced as a new type of ionic liquid. These solvents consist of two or more substances with a melting point lower than their constituents.[17] DESs are typically, but not always, obtained by mixing a quaternary ammonium halide salt, a hydrogen-bond acceptor (HBA) with a hydrogen-bond donor (HBD) molecule, which is capable of forming a complex with the halide, leading to a significant increase in the freezing point.[18] For some compounds, a melting point cannot be detected; hence, a glass transition temperature is obtained instead. Thus, DESs are also known as low-transition-temperature mixtures (LTTMs).[19] As an ionic liquid, DES is not only similar in physical and chemical properties to ionic liquids but also has the advantages of a simple preparation process, low cost, and degradability. Therefore, DESs are

Received: May 23, 2022
Accepted: August 1, 2022
Published: August 9, 2022

https://doi.org/10.1021/acsomega.2c03221
ACS Omega 2022, 7, 29171−29180

widely used in many fields. Additionally, DES has functional gas absorption capacity, especially in the field of air pollution prevention and control.

DESs are more economical alternatives for CO, NH_3, and CO_2 capture and SO_2 and H_2S removal.[20] Wu et al. found that the SO_2 absorption capacities of L-car + EG DES and Bet + EG DES with a mole ratio of 1:3 were 0.820 mol/mol and 0.332 mol/mol at 40 °C, respectively. The results showed that −COO− on Bet and L-car had strong chemical interaction with SO_2.[21] Guo et al. developed tetrabutyl ammonium bromide (TBAB)- and caprolactam-based DESs. They reported that a 1:1 mole ratio exhibited the highest SO_2 absorption capacity, and the DES can be reused for several SO_2 absorption cycles, while it did not have high absorption efficiency.[22] Liu et al. developed a variety of caprolactam-based DESs. The experimental results indicated that the absorption of SO_2 is physical absorption and the solubilities of pure SO_2 of 0.1 MPa in caprolactam-ethanamide DES and caprolactam/imidazole are 0.497 and 0.624 g/g, respectively at 30 °C.[23] In fact, the SO_2 and NO_2 concentrations in the flue gas are very low, and the solubility is too low to have a practical use.

Our previous work showed that NO was mostly physically adsorbed.[24] However, EG-TBAB DES showed the highest NO_2 absorption capacity and can easily be removed. Therefore, the development of environmentally friendly and efficient DESs that can simultaneously absorb low concentrations of SO_2 and NO_2 in the flue gas is of significant importance. One significant advantage of the proposed approach is the generation of high-purity SO_2 and NO_2 during the regeneration of ammonium bromide-type DESs, and the other advantage of the proposed approach is recyclic utilization of the DESs for reducing the cost. In this study, the SO_2 and NO_2 absorption performance and absorption mechanism of the EG-TBAB DESs at different mole ratios of HBA to HBD were systematically investigated at various temperatures and SO_2 partial pressures, and the regeneration experiments of SO_2 and NO_2 were also conducted.

2. EXPERIMENTAL SECTION

2.1. Preparation of Ammonium Bromide-Type DESs. The sample material (ethylene glycol (EG) (AR grade, 99.5%), ethanol (ET) (AR grade, 99.5%), glycerol (GL) (AR grade, 99.5%)), tetraethyl ammonium bromide (TEAB) (AR grade, 99.5%), tetrapropyl ammonium bromide (TPAB) (AR grade, 99.5%), and tetrabutyl ammonium bromide (TBAB) (AR grade, 99.5%) were purchased from Sinopharm Chemical Reagent Co. Ltd. Various types of DESs with different molar ratios were synthesized. The mixtures were stirred at 25 °C for at least 1 h in our previous study.[24,25]

2.2. Characterization of SO_2 and NO_2 Adsorption. The attenuated total reflectance Fourier transform infrared (ATR-FT-IR) spectra were recorded using a Thermo Fisher Nicolet iS5.

^{1}H NMR spectra of DES sample before and after absorption of SO_2 and NO_2 were recorded with a 400 MHz spectrometer (Bruker Avance III, Switzerland) using heavy water (D_2O) as a solvent and tetramethylsilane (TMS) as an internal standard.

The physical properties including the freezing point and melting point were measured by a differential scanning calorimeter (DSC 200 F3).

2.3. Quantum Chemical Calculations of DES Absorption. All of the computational calculations were carried out with Gaussian 16.[26] Quantum chemical calculations of interaction of DESs, SO_2, and NO_2 were performed by the B3LYP method based on density function theory (DFT) at the 6-31G++(d, p) basis set.

2.4. Methods. The SO_2 and NO_2 absorption experiments with ammonium bromide-type DESs were performed using a bubble reactor, under absorption temperatures ranging from 30 to 70 °C; the schematic diagram of the experimental setup is described extensively in our previous study.[24] The simulated flue gas was composed of 0.10 vol % SO_2 and 0.15 vol % NO_2 balanced by N_2. Furthermore, 0−10 vol % O_2 and 5 vol % steam were added when the impact of oxygen presence was investigated. The concentrations of SO_2 and NO_2 at the inlet and outlet of the reactor were monitored by an online flue gas analyzer (MRU MGA5, Germany). The residence time of SO_2 and NO_2 in the glass vessel was observed to be 6 s. The SO_2 and NO_2 desorption experiments were conducted using the same absorption experiment; however, the bubbled gas was changed to pure N_2 and the desorption temperature was increased to 90 °C.

2.5. Data Processing Method. The number of absorbed $SO_2(NO_2)$ (mass ratio of $SO_2(NO_2)$ to DES, desulfurization and denitrification capacity) was determined using eq 1[24,27]

$$m_{SO_2(NO_2)}(\text{mg } SO_2(NO_2)/\text{g DES}) = \frac{M_{DES} \times \rho_{SO_2(NO_2)} \times Q \int_{t_1}^{t_2} (C_o - C_{NO}(t))dt}{m_{DES} \times M_{SO_2(NO_2)}} \quad (1)$$

where $m_{SO_2(NO_2)}$ is the mass absorption capacity of $SO_2(NO_2)$ in EG-TBAB DES, Q (mL/min) is the flow rate of the gas stream, t_1 and t_2 are the starting time of the absorption process and the breakthrough time (i.e., the time at which the $SO_2(NO_2)$ concentration in the outlet stream increased to that in the inlet stream), respectively, m_{DES} is the mass of the DES used for absorption, and $\rho_{SO_2(NO_2)}$ is the density of $SO_2(NO_2)$ under the experimental condition, which is calculated by NIST Refprop software.

The SO_2 (NO_2) absorption efficiency ($\eta(SO_2(NO_2))$) was determined utilizing eq 2

$$\eta((SO_2(NO_2)) = \frac{C_{in} - C_{out}}{C_{in}} \times 100\% \quad (2)$$

where C_{in} and C_{out} are the measured values of SO_2 (NO_2) (ppmv) from the inlet and outlet, respectively.

3. RESULTS AND DISCUSSION

3.1. Melting/Freezing Point of DES. Figure 1 shows that the melting points or the freezing points of EG-TBAB DESs measured by the DSC were much lower than those of the pure constituents at various EG/TBAB molar ratios. Interestingly, the melting points of the EG-TBAB DESs with molar ratios of 4:1 and 5:1 could not be observed at a temperature ranging from −150 to 50 °C. Instead, a glass transition temperature was detected at −120 °C for both mixtures. The molecular structure of the hydrogen-bond donor and receptor, lattice energy, charge distribution, and the strong interaction between ions dictate the melting point of DES.[28] In general, the stronger the interaction between the hydrogen-bond donor and receptor, the higher the destructive force on their crystal structure, hence a high reduction of the melting point degree. To explain the decrease in freezing point in EG/TBAB (5:1) compared to the parent materials, the interactions between the

https://doi.org/10.1021/acsomega.2c03221
ACS Omega 2022, 7, 29171−29180

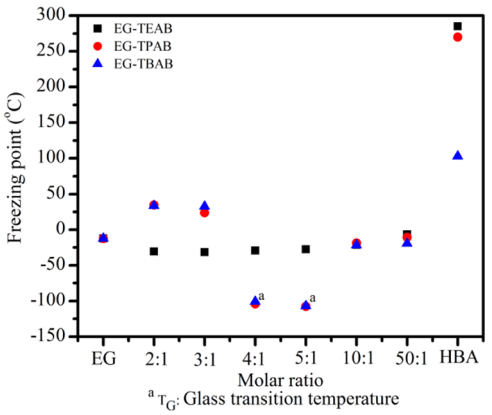

Figure 1. Melting points of the EG-TEAB, EG-TPAB, and EG-TBAB DESs.

ions with each other and the HBD were extensively studied computationally. In addition to the expected BrHN hydrogen bonds, EG also exhibited hydrogen bonding with the bromine cation (e.g., OHNBr), resulting in both Ch-EG and Br-EG clusters. This phenomenon may explain why the eutectic point occurs at 5EG:1TBAB. DESs contain a large number of asymmetric ions, which in turn causes lower lattice energy. The delocalization of charges in hydrogen bonds between halogen ions and HBD is credited for the reduction in the melting point of DES.[29] The larger volume of anions and cations and the conformational flexibility in the DES reduced the lattice enthalpy while increasing the lattice entropy, leading to a decreased lattice free energy (ΔG) and, thus, reducing the melting points.[22] The structure of the cation also played an important role in impacting the melting point of the DESs.

The low glass transition temperature (T_g) also agreed with the results obtained in the literature.[21] As also shown in Figure 1, both the melting point (T_m) and T_g temperature of DESs were noticed. The appearance of T_g indicates that the lattice structure between the hydrogen-bond donor and acceptor was significantly destroyed during the formation of DESs and consequently the crystal structure of pure substances disappeared. It was observed that at temperatures below the T_g temperature, the DESs became glasslike amorphous molten substances. Only glass transition temperatures were detected for EG-TBAB DESs at molar ratios of 4:1 and 5:1, which indicated that at such molar ratios, only glass structures existed and the crystal structures were completely destroyed.

3.2. Effect of HBA on Absorption Performance of SO_2 and NO_2. Figure 2 shows that the simultaneous removal efficiency of SO_2 and NO_x of the DES sample gradually decreased as the reaction time was increased. At 260 min absorption time, it was noticed that the desulfurization and denitrification efficiency of EG-TEAB was extremely reduced and its desulfurization and denitrification effects were no longer noticed. Like EG-TEAB, the desulfurization and denitrification efficiency of EG-TBAB DES after 260 min absorption was also significantly reduced; however, its denitrification efficiency was noted to be slightly better than the desulfurization efficiency. The experimental results showed that the desulfurization and denitrification efficiency of EG-TBAB was significantly better than that of EG-TEAB and EG-TPAB DES, and the simultaneous desulfurization and denitrification efficiency of EG-TBAB DES was the highest among the three DESs. Therefore, with an increase in length of the carbon chain of the quaternary ammonium bromide, the desulfurization and denitrification effect of the binary DES, which was composed of ethylene glycol and quaternary ammonium bromide, showed better absorption properties. This phenomenon can be ascribed to the increase in the carbon chain length, which resulted in a less compact molecular arrangement, thereby creating a large free space; hence, the gas absorption capacity became strong.

The SO_2 and NO_2 absorption capacities of different kinds of ammonium bromide-type DESs were calculated using eq 1 and plotted against the absorption time, as shown in Figure 3. The SO_2 and NO_2 absorption capacity of the DES was noticed to be directly proportional to the carbon chain length of HBA; the highest SO_2 and NO_2 absorption value was achieved with the longest carbon chain of HBA. The desulfurization and denitrification efficiency shown in Figure 1 followed a similar trend, with EG-TBAB DES delivering the highest SO_2 and NO_2 absorption capacity.

In the first 300 min, a rapid increase in the absorption rate for all of the DESs examined was detected. From 0 to 300 min, about 0.18 g SO_2/g DES and 0.252 g NO_2/g DES were absorbed; the process stabilized after 300 min, reaching equilibrium. Figure 3 shows the simultaneous SO_2 and NO_x absorption capacity of different ammonium bromide DESs. The absorption capacity of EG-TBAB DES was higher than that of EG-TEAB and EG-TPAB DES. As a result, EG-TBAB

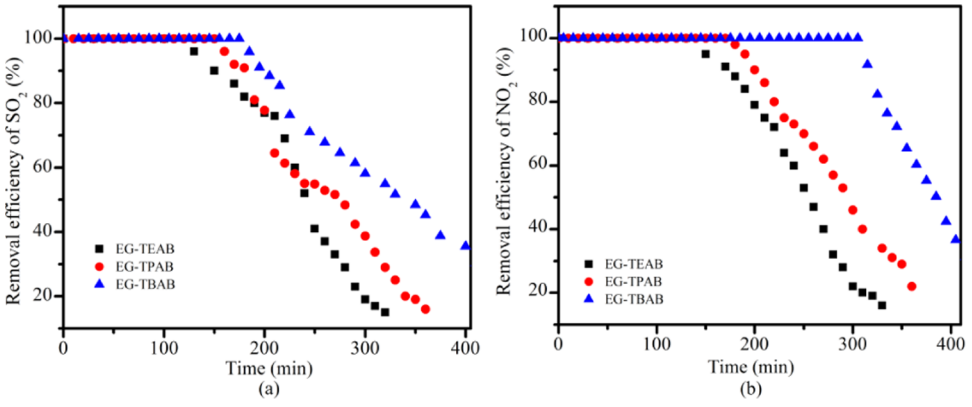

Figure 2. Desulfurization (a) and denitrification efficiency (b) of different ammonium bromide-type DESs (HBD/HBA = 5, At 50 °C with a residence time of 6 s).

https://doi.org/10.1021/acsomega.2c03221
ACS Omega 2022, 7, 29171−29180

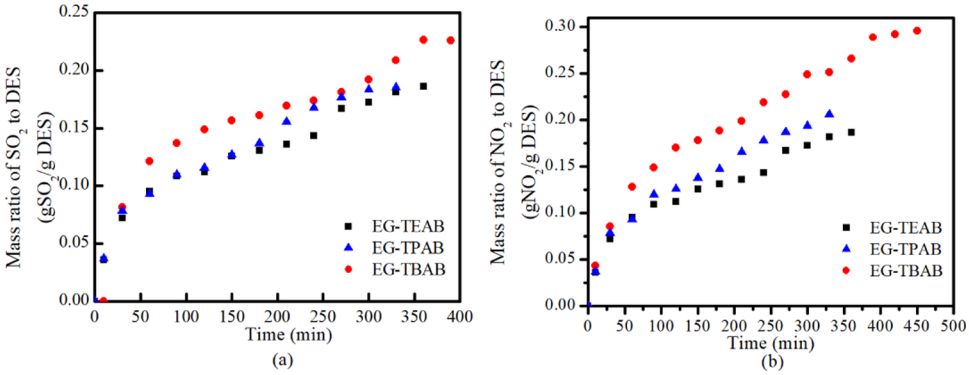

Figure 3. Desulfurization (a) and denitrification capacity (b) of EG-TBAB with different ammonium bromide-type DESs (at 50 °C with a residence time of 6 s).

had the highest desulfurization and denitrification efficiency and also the highest absorption capacity among the ammonium bromide DESs. It can be concluded that EG-TBAB DES effectively removed SO_2 and NO_2 during the desulfurization and denitrification experiments. The SO_2 and NO_2 absorption capacity of EG-TBAB DES was found to be better than that of the other two kinds of DESs (EG-TEAB, EG-TPAB). The desulfurization and denitrification effect of EG-TEAB DES was also better than that of EG-TPAB DES and EG-TEAB DES. It was observed that the stronger the interaction between the hydrogen-bond donor and HBA, the smaller the absorption rate. This result may be attributed to the increase in length of the quaternary ammonium salt carbon chain and the desulfurization and denitrification effect of the binary DES, which was composed of ethylene glycol and tetrabutyl ammonium bromide. At the same time, we also found that the denitrification capacity of DES was better than the desulfurization capacity, which was credited to NO_2 being more polar than SO_2, as it was easier to form a hydrogen bond with Br, SO_2 reacts with N, which is existed in the EG-TBAB and thus more easily removed by it.[23]

3.3. Absorption Mechanism for the Removal of SO_2 and NO_2 by EG-TBAB DES. The ^{1}H NMR spectra of EG-TBAB before and after the absorption process are shown in Figure 4. The typical peaks of the hydrogen atom in TBAB at 3.65, 3.35, and 1.3 ppm, which are associated with the chemical shift of the hydrogen atom connected to C(2) and C(4,5), shifted downward to 1.40 and 3.40 ppm, accordingly. It was also noticed that the $-CH_2-$ peak in the EG shifted upward from 3.65 to 3.70 ppm. This indicates the formation of hydrogen bonds between EG and SO_2/NO_x gas, which may promote SO_2 and NO_2 absorption.[30] The detected peaks all showed a slight change in the height and strength, which is believed to be due to the reaction of SO_2 and NO_2 with OH···Br$^-$.

Figure 5 shows the Fourier transform infrared (FT-IR) spectra of EG-TBAB DES before and after the absorption reaction. The peaks in the range of 4000−2000cm^{-1}, associated with functional groups, remained unchanged before and after the reaction; FT-IR peaks located in ranges of 1545−1570, 700−900, ∼1610, and 1560−1490 cm^{-1} that were associated with the aromatic ring C═C, aromatic C−H groups, and aromatic carbon and stretched aromatic rings were recorded for all samples.[31] From Figure 5, the new absorption peaks appearing in the spectrum for the SO_2-saturated EG-TBAB DES at 1321 (vs S═O) were assigned to the symmetrical stretching vibration of (vs S═O) and could be a result of the physical absorption of SO_2. The peaks at 1650 and 1350 cm^{-1} could be assigned to N−O stretching vibrations.[32] The above results showed that the oxygen of EG-TBAB physically interacts with SO_2/NO_2 and suggested the presence of dual-site chemical N···SO_2 and O···SO_2 interactions, which lead to the improvement of NO_2 and SO_2 chemisorption by EG-TBAB DESs. SO_2 molecules reacted with N−H in cations to form N−S bonds, and the acid ions formed corresponding acids; the N−S bond was reversible;

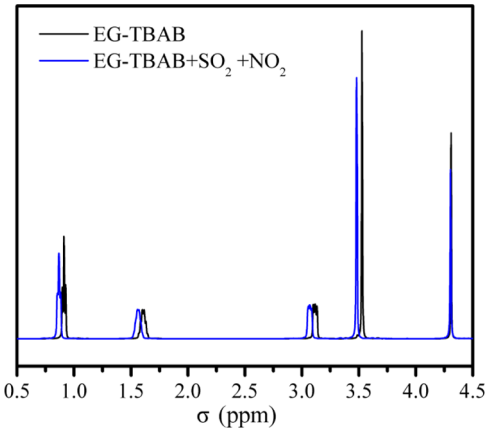

Figure 4. ^{1}H NMR spectra of EG-TBAB DES before and after absorption.

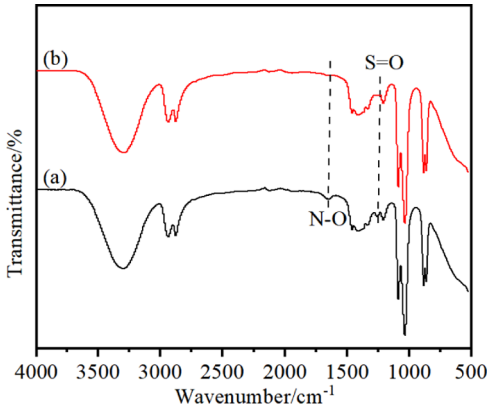

Figure 5. FT-IR spectra of EG-TBAB DES before (a) and after (b) desulfurization and denitrification.

https://doi.org/10.1021/acsomega.2c03221
ACS Omega 2022, 7, 29171−29180

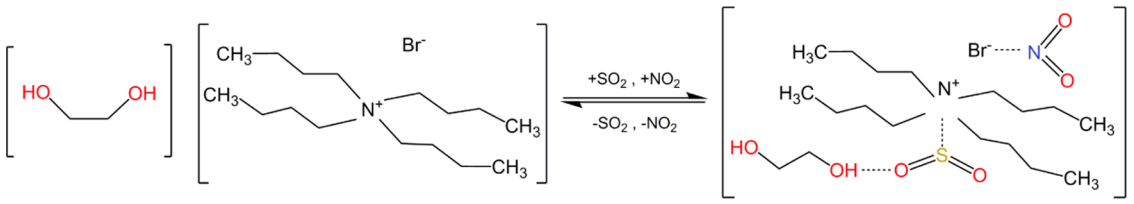

Figure 6. Mechanism diagram of the SO_2 and NO_2 removal process with ammonium bromide DES for flue gas cleaning.

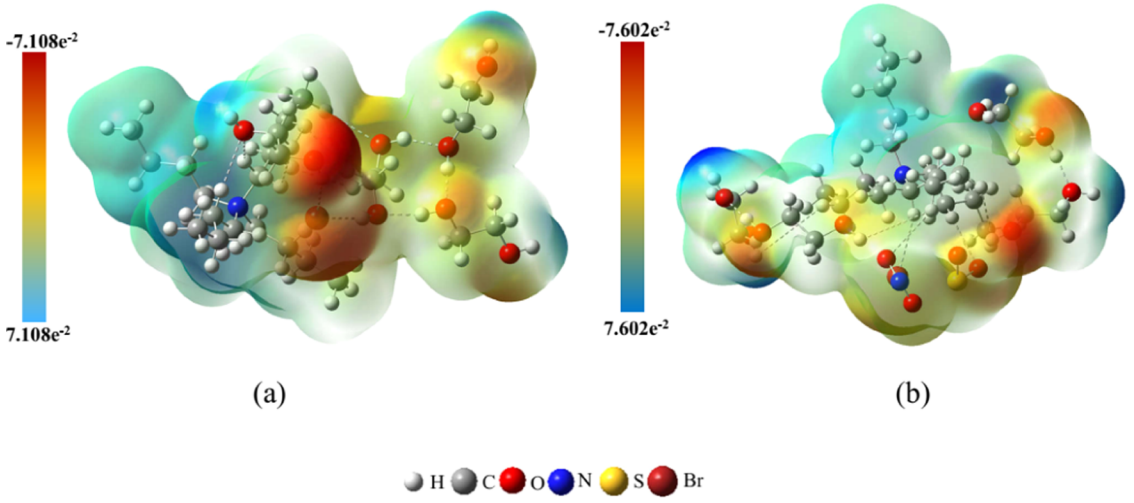

Figure 7. Optimized structure of complexes (a) EG-TBAB DESs and (b) EG-TBAB DESs with SO_2 and NO_2.

under heating or vacuum conditions, the N−S bond could break and release SO_2. The DES could be regenerated and reused. The reaction mechanism is shown in Figure 6. From ^{1}H NMR and FT-IR spectra, it could be concluded that NO_2 is primarily chemically absorbed in the case of EG-TBAB. SO_2 and NO_2 were absorbed by forming the EG-TBAB-SO_2−NO_2 complexes in the DES, and this complexing interaction did break the chemical structure of EG-TBAB DES.

3.4. Quantum Chemical Calculations of SO_2 and NO_2 Absorption by EG-TBAB DES. Computational studies were carried out to fundamentally investigate the interaction between the elemental component of EG-TBAB DES and SO_2/NO_2. Figure 7 shows the lowest-energy structures found for the EG-TBAB DES ion pair interacting with SO_2 and NO_2 gas contaminants. This was done by studying the geometry optimizations from different initial structures; several slightly different low-energy EG-TBAB DES-SO_2−NO_2 structures are produced. However, all of the structures consist of an EG O atom forming a H-bond with the H at C_2 on TBAB, and the X atom in the XO_2 absorbate is attracted noncovalently toward one of the EG O atoms. Table 1 summarizes the optimized X−O EG-TBAB DES and TBAB H−O EG distances and also lists the XO_2 absorption enthalpy (ΔH) and Gibbs energy (ΔG) with EG-TBAB at 298 K. As expected, SO_2 and NO_2 had small binding enthalpies with EG-TBAB DES compared to SO_2, which correlates to the large decrease in the X−O EG bonding distance as the X binding strength increases. At the same time, the strong bond of SO_2 reduces the H-bonding interaction between TBAB and EG as reflected by the longer EG O−H TBAB bonding distances of these two molecules. Finally, the ΔG values suggest that NO_2 can readily bind with EG-TBAB DES. These results correlate well with the experimental results observed for the single gas contaminant sorption by EG-TBAB DES, which had a higher breakthrough time and capacity for NO_2 sorption compared to that for SO_2 and NO_2. However, the ΔH and ΔG binding energies of EG-TBAB NO_2 were different from those computed for the SO_2 and NO_2 adsorbed on EG-TBAB, suggesting that the NO_2 interaction is not strongly influenced by the presence of SO_2. The adsorption energy (ΔH and ΔG) of the additional SO_2 was slightly lower comparing to the initial SO_2 adsorption energy on EG-TBAB. The increase in bond length of N−O EG-TBAB from 2.514 Å in EG-TBAB·NO_2 to 2.604 Å in EG-TBAB·NO_2−SO_2 suggests that the NO_2 interaction with EG-TBAB was weakened by SO_2 adsorption. This is in direct correlation with the simulated gas contaminant breakthrough data for EG-TBAB, which indicates an abrupt overshoot of NO_2 at the outlet as SO_2 begins to break through (Figure 7b). The breakthrough curve data suggest that there are preferential binding sites on deep eutectic solvents for NO_2 and SO_2. However, once the SO_2-preferred binding sites are filled, SO_2 begins to occupy the NO_2 sites due to the larger binding energies for SO_2 than those for NO_2 by the EG-TBAB DES. Furthermore, after initial SO_2 adsorption by EG-TBAB, the adsorption energies for either NO_2 or SO_2 will be significantly reduced. A careful selection of the DES cation or a combination of the DES with other DES should enable fine-tuning of the adsorption properties for the

Table 1. Optimized X−O EG-TBAB DES and TBAB H−O EG Distances; SO_2, NO_2, and SO_2 and NO_2 Interaction Energy (ΔE); Absorption Enthalpy (ΔH); and Gibbs Energy (ΔG) with EG-TBAB at 298 K

structural parameters	DES-SO_2	DES-NO_2	DES-SO_2−NO_2
ΔE (kJ/mol)	−101.2	−110.8	−98.8
ΔH (kJ/mol)	−124.2	−135.7	−153.4
ΔG (kJ/mol)	−10.5	−30.6	−32.5

https://doi.org/10.1021/acsomega.2c03221
ACS Omega 2022, 7, 29171−29180

DES anion, thus enabling reversible and selective absorption of SO_2 and NO_2.[33]

Table 2 illustrates the structural parameters of the optimized geometries before and after SO_2 and NO_2 absorption. The organization of gas molecules around the anion is related to absorption. As shown in Table 2, the average O−N−O angle bends from 179.98 to 116.09° and the average O−S−O angle bends from 116.24 to 134.05°. The angle change for NO_2 was more pronounced in an EG-TBAB-NO_2−SO_2 complex than that for SO_2. Bromide anions in the EG-TBAB DES maintained strong interactions with NO_2 via hydrogen bonding, leading to increased NO_2 adsorption in our previous study.[24,25] This result further indicated that NO_2 was primarily absorbed by the Br anion site in EG-TBAB DES, and NO_2 interaction with EG-TBAB is easier compared to SO_2.

Table 2. Structural Parameters of EG-TBAB DESs before and after SO_2 and NO_2 Absorption

structural parameters	SO_2	NO_2	DES-SO_2−NO_2	Δ
O−N−O (°)		179.98	116.09	63.89
O−S−O (°)	116.24		134.05	−17.81

3.5. Effect of Operation Temperature on the Desulfurization and Denitrification Performance of DES. Figure 8 demonstrates the desulfurization and denitrification capacity of DES vs temperature. The SO_2 and NO_2 absorption of fresh DES increased with the temperature increasing from 30 to 50 °C. At 50 °C, the SO_2 and NO_2 absorption capacities of DESs were 0.226 g SO_2/g DES and 0.296 g NO_2/g DES, respectively, which were much higher than 0.12 g SO_2/g DES and 0.07 g NO_2/g DES (Figure 8). The simultaneous desulfurization and denitrification capacity at 50 °C was significantly better than that at 30°C and 70°C. The results show that maintaining an appropriate absorption temperature is critical to achieving high absorption capacity, and high temperature negatively impacted the adsorption of SO_2 and NO_2. This observation may result from the temperature-independent viscosity effect. During SO_2 and NO_2 absorption, viscosity affects the transfer of mass greatly,[34] and especially, DESs are typically high-viscosity solvents. When the temperature increases, the molecular motion in the system of the SO_2, NO_2, and DES intensifies, leading to an increase in the saturated vapor pressure of SO_2 and NO_2, resulting in the breaking of the intermolecular forces, leaving SO_2 and NO_2 to easily escape from the DESs, and correspondingly decreasing the SO_2 and NO_2 absorption rate.

3.6. Effect of the Molar Ratio of EG to TBAB on the Desulfurization and Denitrification Performance of DESs. The absorption capacity of SO_2 and NO_2 by DESs with different molar ratios is shown in Figure 9. It was observed that the molar ratio of HBA to HBD composites in DES influenced the desulfurization and denitrification capacity of DES. This is possibly related to various intermolecular behaviors with DESs consisting of different EG:TBAB ratios. When the EG:TBAB ratio was lower than 5:1, the parent TBAB salt ions and HBD molecules in the DES systems were more likely to interact with each other through the electrostatic and H-bonding interactions, thus showing weaker affinities for SO_2 and NO_2 molecules and leading to lower desulfurization and denitrification efficiency and absorption capacity. However, when the EG:TBAB ratio was higher than 10:1, the concentration of EG was believed to be at a point where the system had lost the DES physicochemical properties and acted as a solution with TBAB salt dissolved in EG. The anion−HBD interaction force was significantly destroyed at such molar ratios, leading to a reduced H-bonding network between the HBD and ions and thus resulting in a reduced SO_2 and NO_2 absorption capacity.

3.7. Effect of Oxygen and Steam on the Desulfurization and Denitrification Performance of DES. Figure 10 shows the absorption capacity of SO_2 and NO_2 with different oxygen and steam concentrations in the simulated flue gas. To understand the effect of oxygen content in flue gas on the desulfurization and denitrification capacity of EG-TBAB DES, different oxygen partial pressures ranging from 0 to 10% were studied. Figure 10 shows that in the absence of oxygen and steam, the desulfurization and denitrification capacity of DES was the lowest. As the oxygen and steam partial pressure increased to 5%, the SO_2/NO_2 adsorption capacity of the developed DES was significantly increased. Therefore, it can be concluded that oxygen and steam had a promotion effect on the desulfurization and denitrification capacity during the simultaneous desulfurization and denitrification process of EG-TBAB DES, which was possibly due to the natural affinity between the polar H_2O, SO_2, and NO_2 molecules. SO_2 and NO_2 can react with O_2 and H_2O to form HNO_3 at low reaction temperatures, as shown in eqs 3−7.

$$SO_2(g) + DES(l) \rightarrow DES - SO_2(l) \quad (3)$$

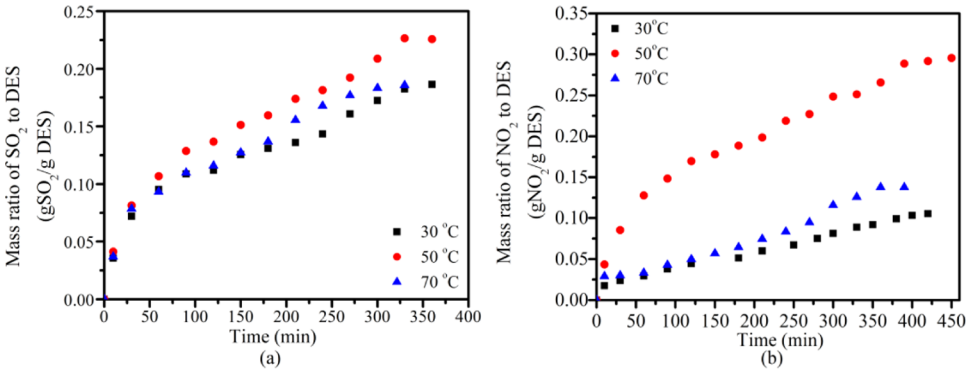

Figure 8. Desulfurization (a) and denitrification capacity (b) of EG-TBAB DESs at different operation temperatures (at an EG to TBAB molar ratio of 5:1 and a residence time of 6 s).

https://doi.org/10.1021/acsomega.2c03221
ACS Omega 2022, 7, 29171−29180

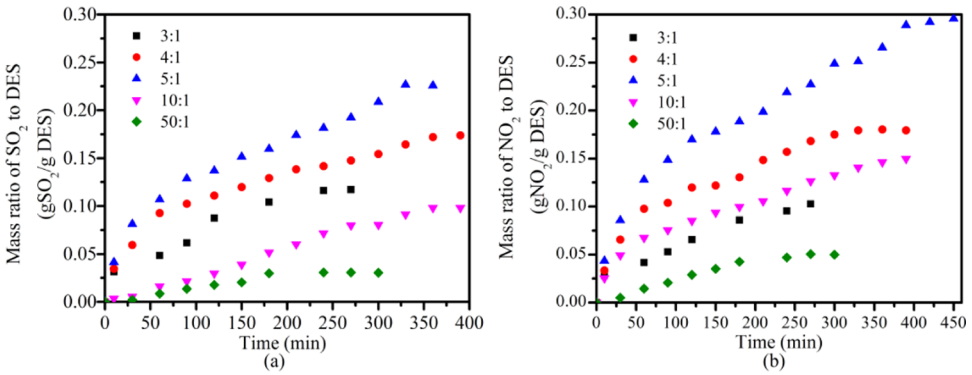

Figure 9. Desulfurization (a) and denitrification capacity (b) of DES with different EG to TBAB molar ratios (at 50 °C with a residence time of 6 s).

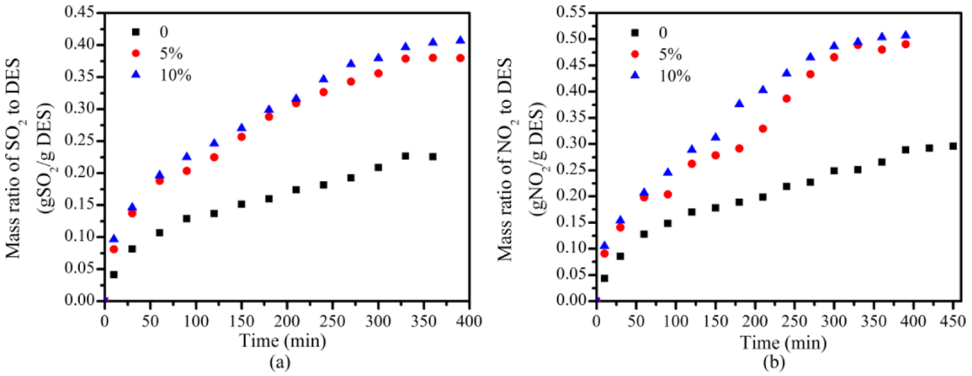

Figure 10. Desulfurization (a) and denitrification capacity (b) of DES at different steam concentrations (at 50 °C with a residence time of 6 s).

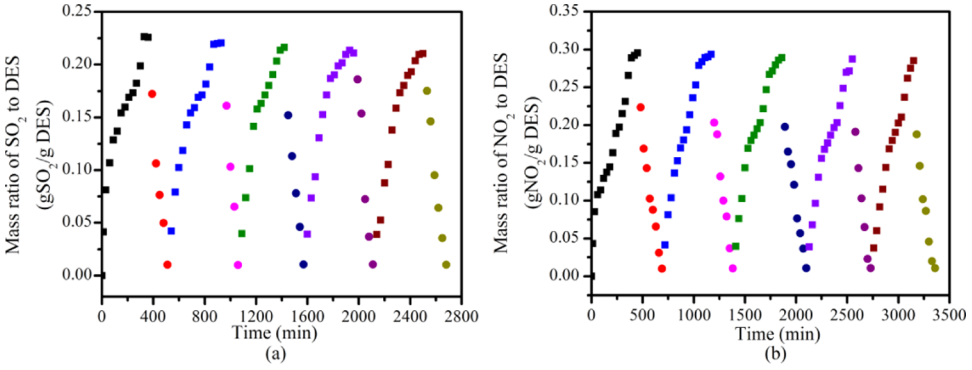

Figure 11. Desulfurization (a) and denitrification capacity (b) of DES during five absorption−desorption cycles (desorption temperature at 100 °C and a gas flow of 100 mL/min).

$$NO_2(g) + DES(l) \rightarrow DES - NO_2(l) \quad (4)$$

$$H_2O(g) + DES(l) \rightarrow DES - H_2O(l) \quad (5)$$

$$O_2(g) + DES(l) \rightarrow DES - O_2(l) \quad (6)$$

$$DES - O_2(l) + DES - SO_2(l) + DES - NO_2(l) + DES - H_2O(l) \rightarrow DES - H_2SO_4(l) + DES - HNO_3(l) \quad (7)$$

The results proved that the EG-TBAB DES had a high capacity to absorb the generated HNO_3 and H_2SO_4.[35] However, in the presence of steam (10% concentration), the desulfurization and denitrification capacity was not obviously increased. The results further indicated that the presence of steam can effectively promote SO_2 and NO_2 absorption of DES. This result was attributed to the high viscosity of DES, which is not conducive to mass transfer, thus affecting the absorption rate and efficiency of SO_2 and NO_2 when steam exists in the flue gas. It was found that the viscosity of the DES was reduced, while its absorption capacity did not decline. Therefore, the presence of steam is highly conducive to SO_2 and NO_2 absorption.[36,37]

3.8. Regeneration Performance of EG-TBAB DES. Absorption/desorption process reversibility is a major criterion for industrial solvents. SO_2 and NO_2 desorption and recycling of EG-TBAB DES were investigated in this study, and the experimental findings are displayed in Figure 11. SO_2 and NO_2 absorbed by EG-TBAB DES can easily be separated from the solvent by bubbling N_2 at 100 °C within 60 min, indicating a simple desorption process of SO_2 and NO_2. This observation

https://doi.org/10.1021/acsomega.2c03221
ACS Omega 2022, 7, 29171−29180

Table 3. Comparison with Other DESs from the Literature under Low Partial Pressures of SO_2 and NO_2[ab]

absorbents	T (°C)	C_{SO_2} (%) and C_{NO_2} (%) in volume fraction	absorption capacity of SO_2	absorption capacity of NO_2[c]	refs
EG-TEAB	50	0.1, 0.15	0.186	0.186	this work
EG-TPAB	50	0.1, 0.15	0.186	0.206	this work
EG-TBAB	50	0.1, 0.15	0.226	0.296	this work
Im-H_2O	40	0.2	0.267[c]		38
[P4442][Tetz]	20	0.2	0.190[c]		39
EmimCl-NFM	20	0.2	0.135[c]		40
PPZBr-Gly (1:6)	20	0.1	0.130[c]		41
[E_2Py]Cl	20	20	1.155[c]		42
Bisazole-based DESs	20	0.1	1.402[c]		43
EmimCl-EPyBr (3:1)	20	0.1	0.698[c]		44
TBAB-CPL DESs	20	0.1	0.764[c]		45

[a]In units of grams of NO_2 per gram of DES. [b]In units of grams of SO_2 per gram of DES. [c]In units of grams of SO_2 per gram of IL.

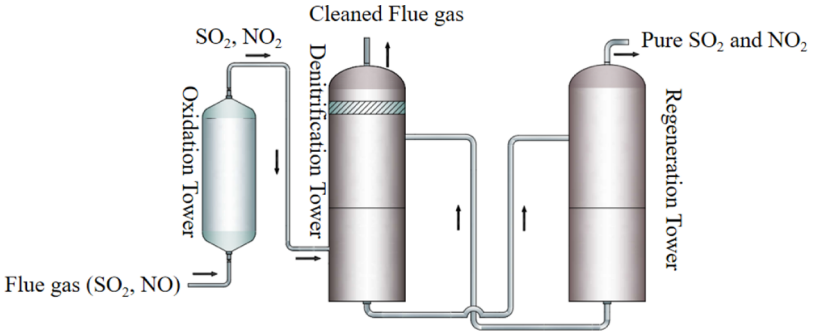

Figure 12. Schematic diagram of the SO_2 and NO_2 removal process by ammonium bromide DES for flue gas cleaning.

indicates that very low energy costs are required for the regeneration process of the DES. Evidently, the EG-TBAB DES exhibited good absorption/desorption behavior, the absorption capacity/desorption time was well maintained, and the SO_2 and NO_2 absorption capacity during the five recycling cycles remained relatively unchanged. The stability of these five absorption/desorption cycles makes EG-TBAB DES a promising solvent, which is green, cheap, and renewable, for the absorption of SO_2 and NO_2.

3.9. Comparison of the SO_2 and NO_2 Absorption Capacities of the Absorbent Investigated in This Study with Those in the Literature. The SO_2 and NO_2 absorption capacities of the absorbent used in this study and those found in the literature are given in Table 3. Table 3 shows that the absorption capacity of SO_2 of various solvents under different experimental conditions varies significantly. Compared to other DESs, this absorbent can absorb both SO_2 and NO_2. For instance, the absorption capacity of SO_2 and NO_2 of EG-TBAB DES at 50 °C was 0.226 g for SO_2/g and 0.296g for NO_2/g DES, which is the highest among all of the absorbents. This indicates that the absorbent developed in this work has a great potential to be implemented industrially.

3.10. Implications of Denitrification and Desulfurization Technology. A schematic diagram for the removal of SO_2 and NO_2 using ammonium bromide DES is shown in Figure 12. During the denitrification process, NO was first converted to NO_2 using vaporized O_3-based peroxide complex oxidants, followed by SO_2 and NO_2 removal in the flue gas absorption tower using EG-TBAB DESs; the cleaned flue gas then entered the atmosphere through a stack. In the regeneration tower, high-purity SO_2 and NO_2 released from the sorbent were collected for other applications; the regenerated EG-TBAB DESs could be reused and recycled for the next SO_2 and NO_2 absorption process. As can be seen from Table S1, the overall energy consumption of this process unit is 9.86 RMB/t coke. This cost is higher than conventional desulfurization and denitrification technology due to the separation and recovery of DES, which consumes energy; the price of DES is also higher compared to other absorbents. However, the recovery of EG-TBAB DES mainly depends on the reverse extraction of water; the evaporation of water consumes too much energy.

4. CONCLUSIONS

In this study, ethylene glycol and different length ammonium bromide carbon chains (tetraethyl ammonium bromide, tetrapropyl ammonium bromide, and tetrabutyl ammonium bromide) were used to prepare deep eutectic solvents. The experimental results showed that the best desulfurization and denitrification performance of DES was achieved at 50 °C absorption temperature and a TBAB:EG molar ratio of 5. ^{1}H NMR results showed that the EG-TBAB DESs successfully removed SO_2 and NO_2. Oxygen was noticed to inhibit the absorption performance of the EG-TBAB DES, while steam promoted the absorption performance of the EG-TBAB DES. The absorption process mechanism in the presence of steam was found to be due to the combination of both chemical absorption and physical absorption, while in the absence of steam, the mechanism of the reaction was mainly due to physical absorption. The quantum chemical calculations of DES absorption indicated that NO_2 was more pronounced in an EG-TBAB-NO_2−SO_2 complex than SO_2, the Br anion in EG-TBAB DES was the primary active site for NO_2 absorption, and NO_2 could easily interact with EG-TBAB than SO_2. The regeneration experiments confirmed that DES had excellent regeneration performance, and the SO_2 and NO_2 absorption

https://doi.org/10.1021/acsomega.2c03221
ACS Omega 2022, 7, 29171−29180

capacities of the DES did not change during the five absorption−desorption cycles conducted.

■ ASSOCIATED CONTENT

Supporting Information

The Supporting Information is available free of charge at https://pubs.acs.org/doi/10.1021/acsomega.2c03221.

(Experiment) Preparation of ammonium bromide-type DESs and quantum chemical calculations of DES absorption and (Table S1) production energy consumption (PDF)

■ AUTHOR INFORMATION

Corresponding Authors

Jinxiao Dou − *Key Laboratory of Advanced Coal and Coking Technology of Liaoning Province, School of Chemical Engineering, University of Science and Technology Liaoning, Anshan 114051, China*; Phone: +86-(0)412-5929105; Email: doujx123@163.com

Jianglong Yu − *Key Laboratory of Advanced Coal and Coking Technology of Liaoning Province, School of Chemical Engineering, University of Science and Technology Liaoning, Anshan 114051, China; Suzhou Industrial Park Monash Research Institute of Science and Technology; and Southeast University-Monash University Joint Graduate School, Suzhou 215123, China*; orcid.org/0000-0002-5932-0813; Phone: +86-(0)512-62997871; Email: jianglong.yu@monash.edu

Authors

Tengteng Zhou − *Key Laboratory of Advanced Coal and Coking Technology of Liaoning Province, School of Chemical Engineering, University of Science and Technology Liaoning, Anshan 114051, China*

Yongqi Zhao − *Key Laboratory of Advanced Coal and Coking Technology of Liaoning Province, School of Chemical Engineering, University of Science and Technology Liaoning, Anshan 114051, China*

Xinxin Xiao − *Key Laboratory of Advanced Coal and Coking Technology of Liaoning Province, School of Chemical Engineering, University of Science and Technology Liaoning, Anshan 114051, China*

Yixuan Liu − *Key Laboratory of Advanced Coal and Coking Technology of Liaoning Province, School of Chemical Engineering, University of Science and Technology Liaoning, Anshan 114051, China*

Hongcun Bai − *State Key Laboratory of High-efficiency Utilization of Coal and Green Chemical Engineering, Ning Xia University, Yinchuan 750021, China*

Xingxing Chen − *Key Laboratory of Advanced Coal and Coking Technology of Liaoning Province, School of Chemical Engineering, University of Science and Technology Liaoning, Anshan 114051, China*

Complete contact information is available at: https://pubs.acs.org/10.1021/acsomega.2c03221

Author Contributions

‖

T.Z. and Y.Z. contributed equally to this work.

Notes

The authors declare no competing financial interest.

■ ACKNOWLEDGMENTS

This work was supported by funding from the Natural Science Foundation of Liaoning Province (2022-MS-374), the Excellent Talents Training Program of the University of Science and Technology Liaoning (2019RC12), the Education Department Excellent Talents Training Program of Liaoning Province (2020LNQN21), Liaoning High-Level Innovation Team Overseas Training Project (2018LNGXGJWPY-YB010), the Foundation of the State Key Laboratory of High-efficiency Utilization of Coal and Green Chemical Engineering (2022-K77), and the International Collaborative Centre for Carbon Futures.

■ REFERENCES

(1) Huo, W. C.; Dong, X. a.; Li, J. Y.; Liu, M.; Liu, X. Y.; Zhang, Y. X.; Dong, F. Synthesis of Bi_2WO_6 with gradient oxygen vacancies for highly photocatalytic NO oxidation and mechanism study. *Chem. Eng. J.* **2019**, *361*, 129−138.

(2) Mao, F.-F.; Zhou, Y.; Zhu, W.; Sang, X.-Y.; Li, Z.-M.; Tao, D.-J. Synthesis of Guanidinium-Based Poly(ionic liquids) with Nonporosity for Highly Efficient SO_2 Capture from Flue Gas. *Ind. Eng. Chem. Res.* **2021**, *60*, 5984−5991.

(3) Tao, D.-J.; Qu, F.; Li, Z.-M.; Zhou, Y. Promoted absorption of CO at high temperature by cuprous-based ternary deep eutectic solvents. *AIChE J.* **2021**, *67*, No. e17106.

(4) Liu, X.; Zhou, Y.; Wang, C.-L.; Liu, Y.; Tao, D.-J. Solvent-free self-assembly synthesis of N-doped ordered mesoporous carbons as effective and bifunctional materials for CO_2 capture and oxygen reduction reaction. *Chem. Eng. J.* **2022**, *427*, No. 130878.

(5) Gupta, A. K.; Ibrahim, S.; Al Shoaibi, A. Advances in sulfur chemistry for treatment of acid gases. *Prog. Energy Combust. Sci.* **2016**, *54*, 65−92.

(6) Liu, Y.; Shi, S.; Wang, Z. A novel double metal ions-double oxidants coactivation system for NO and SO_2 simultaneous removal. *Chem. Eng. J.* **2022**, *432*, No. 134398.

(7) Wang, Y.; Liu, Y.; Shi, S. Removal of nitric oxide from flue gas using novel microwave-activated double oxidants system. *Chem. Eng. J.* **2020**, *393*, No. 124754.

(8) Bergman, S. L.; Granestrand, J.; Tang, Y.; París, R. S.; Nilsson, M.; Tao, F. F.; Tang, C.; Pennycook, S. J.; Pettersson, L. J.; Bernasek, S. L. In-situ characterization by Near-Ambient Pressure XPS of the catalytically active phase of Pt/Al_2O_3 during NO and CO oxidation. *Appl. Catal., B* **2018**, *220*, 506−511.

(9) Pena-Pereira, F.; Namieśnik, J. Ionic Liquids and Deep Eutectic Mixtures: Sustainable Solvents for Extraction Processes. *ChemSusChem* **2014**, *7*, 1784−1800.

(10) Ma, S.; Shang, X.; Li, J.; Li, L.; Sun, Y.; Yang, Y.; Sun, L. Liquid−Liquid Extraction of Benzene Using Low Transition Temperature Mixtures: COSMO-SAC Predictions and Experiments. *J. Chem. Eng. Data* **2018**, *63*, 4749−4760.

(11) Emel'yanenko, V. N.; Boeck, G.; Verevkin, S. P.; Ludwig, R. "Volatile times for the very first ionic liquid: Understanding the vapor pressures and enthalpies of vaporization of ethylammonium nitrate",. *Chem. - Eur. J.* **2014**, *20*, 11640−11645.

(12) Meine, N.; Benedito, F.; Rinaldi, R. Thermal stability of ionic liquids assessed by potentiometric titration. *Green Chem.* **2010**, *12*, 1711−1714.

(13) Maton, C.; De Vos, N.; Stevens, C. V. Ionic liquid thermal stabilities: decomposition mechanisms and analysis tools. *Chem. Soc. Rev.* **2013**, *42*, 5963−5977.

(14) Fox, D. M.; Gilman, J. W.; Morgan, A. B.; Shields, J. R.; Maupin, P. H.; Lyon, R. E.; De Long, H. C.; Trulove, P. C. Flammability and Thermal Analysis Characterization of Imidazolium-Based Ionic Liquids. *Ind. Eng. Chem. Res.* **2008**, *47*, 6327−6332.

(15) Li, X.; Zhang, L.; Zheng, Y.; Zheng, C. Effect of SO_2 on CO_2 Absorption in Flue Gas by Ionic Liquid 1-Ethyl-3-methylimidazolium Acetate. *Ind. Eng. Chem. Res.* **2015**, *54*, 8569−8578.

(16) Zhang, X.; Zhang, X.; Dong, H.; Zhao, Z.; Zhang, S.; Huang, Y. Carbon capture with ionic liquids: overview and progress. *Energy Environ. Sci.* **2012**, *5*, 6668−6681.
(17) Biczak, R.; Pawłowska, B.; Bałczewski, P.; Rychter, P. The role of the anion in the toxicity of imidazolium ionic liquids. *J. Hazard. Mater.* **2014**, *274*, 181−190.
(18) Thuy Pham, T. P.; Cho, C. W.; Yun, Y. S. Environmental fate and toxicity of ionic liquids: a review. *Water Res.* **2010**, *44*, 352−372.
(19) Peric, B.; Sierra, J.; Martí, E.; Cruañas, R.; Garau, M. A.; Arning, J.; Bottin-Weber, U.; Stolte, S. (Eco)toxicity and biodegradability of selected protic and aprotic ionic liquids. *J. Hazard. Mater.* **2013**, *261*, 99−105.
(20) Smiglak, M.; Reichert, W. M.; Holbrey, J. D.; Wilkes, J. S.; Sun, L.; Thrasher, J. S.; Kirichenko, K.; Singh, S.; Katritzky, A. R.; Rogers, R. D. Combustible ionic liquids by design: is laboratory safety another ionic liquid myth? *Chem. Commun.* **2006**, 2554−2556.
(21) Hou, Y. C.; Yao, C. F.; Wu, W. Z. Deep Eutectic Solvents: Green Solvents for Separation Applications. *Acta Phys.-Chim. Sin.* **2018**, *34*, 873−885.
(22) Chen, Y.; Han, X.; Liu, Z.; Yu, D.; Guo, W.; Mu, T. Capture of Toxic Gases by Deep Eutectic Solvents. *ACS Sustainable Chem. Eng.* **2020**, *8*, 5410−5430.
(23) Liu, B.; Zhao, J.; Wei, F. Characterization of caprolactam based eutectic ionic liquids and their application in SO_2 absorption. *J. Mol. Liq.* **2013**, *180*, 19−25.
(24) Dou, J. X.; Zhao, Y. Q.; Yin, F. K.; Li, H.; Yu, J. L. Mechanistic Study of Selective Absorption of NO in Flue Gas Using EG-TBAB Deep Eutectic Solvents. *Environ. Sci.Technol.* **2019**, *53*, 1031−1038.
(25) Dou, J. X.; Zhao, Y. Q.; Li, H.; Wang, J. P.; Tahmasebi, A.; Yu, J. L. Mechanistic Study on the Removal of NO_2 from Flue Gas Using Novel Ethylene Glycol-tetrabutylammonium Bromide Deep Eutectic Solvents. *ACS Omega* **2020**, *5*, 31220−31226.
(26) Caricato, M.; Frisch, M. J.; Hiscocks, J.; Frisch, M. J. Gaussian 09: Iops reference, Citeseer, 2009.
(27) Carriazo, D.; Serrano, M. C.; Gutiérrez, M. C.; Ferrer, M. L.; del Monte, F. Deep-eutectic solvents playing multiple roles in the synthesis of polymers and related materials. *Chem. Soc. Rev.* **2012**, *41*, 4996−5014.
(28) Cui, G.; Jiang, K.; Liu, H.; Zhou, Y.; Zhang, Z.; Zhang, R.; Lu, H. Highly efficient CO removal by active cuprous-based ternary deep eutectic solvents [HDEEA][Cl] + CuCl + EG. *Sep. Purif. Technol.* **2021**, *274*, No. 118985.
(29) Deng, D.; Deng, X.; Duan, X.; Gong, L. Protic guanidine isothiocyanate plus acetamide deep eutectic solvents with low viscosity for efficient NH_3 capture and NH_3/CO_2 separation. *J. Mol. Liq.* **2020**, *324*, No. 114719.
(30) Zhao, Y. Q.; Dou, J. X.; Wei, A. R.; Khoshkrish, S.; Yu, J. L. Highly efficient and reversible low-concentration SO_2 absorption in flue gas using novel phosphonium-based deep eutectic solvents with different substituents. *J. Mol. Liq.* **2021**, *340*, No. 117228.
(31) Tahmasebi, A.; Yu, J.; Han, Y.; Yin, F.; Bhattacharya, S.; Stokie, D. Study of Chemical Structure Changes of Chinese Lignite upon Drying in Superheated Steam, Microwave, and Hot Air. *Energy Fuels* **2012**, *26*, 3651−3660.
(32) Chen, K.; Shi, G.; Zhou, X.; Li, H.; Wang, C. Highly Efficient Nitric Oxide Capture by Azole-Based Ionic Liquids through Multiple-Site Absorption. *Angew. Chem., Int. Ed.* **2016**, *55*, 14364−14368.
(33) Zeng, S.; Zhang, X.; Gao, H.; He, H.; Zhang, X.; Zhang, S. SO_2-Induced Variations in the Viscosity of Ionic Liquids Investigated by in Situ Fourier Transform Infrared Spectroscopy and Simulation Calculations. *Ind. Eng. Chem. Res.* **2015**, *54*, 10854−10862.
(34) Krossing, I.; Slattery, J. M.; Daguenet, C.; Dyson, P. J.; Oleinikova, A.; Weingärtner, H. Why are ionic liquids liquid? A simple explanation based on lattice and solvation energies. *J. Am. Chem. Soc.* **2006**, *128*, 13427−13434.
(35) Chen, Z.; Greaves, T. L.; Warr, G. G.; Atkin, R. Mixing cations with different alkyl chain lengths markedly depresses the melting point in deep eutectic solvents formed from alkylammonium bromide salts and urea. *Chem. Commun.* **2017**, *53*, 2375−2377.
(36) Yuan, X. L.; Zhang, S.; Lu, X. Hydroxyl Ammonium Ionic Liquids: Synthesis, Properties, and Solubility of SO_2. *J. Chem. Eng. Data* **2007**, *52*, 596−599.
(37) Duan, E.; Guo, B.; Zhang, D.; Shi, L.; Sun, H.; Wang, Y. Absorption of NO and NO_2 in caprolactam tetrabutyl ammonium halide ionic liquids. *J. Air Waste Manage. Assoc.* **2011**, *61*, 1393−1397.
(38) Gao, M.; Hou, Y.; Zhang, Q.; Sun, Y.; Ren, S.; Wu, W. Absorption of SO_2 in Simulated Flue Gas by Functional Deep Eutectic Solvents Based on Imidazole and H_2O with High Mass Capacities. *Energy Fuels* **2020**, *34*, 4754−4760.
(39) Che, S.; Dao, R.; Zhang, W.; Lv, X.; Li, H.; Wang, C. Designing an anion-functionalized fluorescent ionic liquid as an efficient and reversible turn-off sensor for detecting SO_2. *Chem. Commun.* **2017**, *53*, 3862−3865.
(40) Deng, D.; Zhang, C.; Deng, X.; Gong, L. Efficient absorption of low partial pressure SO_2 by 1-ethyl-3-methylimidazolium chloride plus N-formylmorpholine deep eutectic solvents. *Energy Fuels* **2020**, *34*, 665−671.
(41) Cui, G.; Liu, J.; Lyu, S.; Wang, H.; Li, Z.; Wang, J. Efficient and reversible SO_2 absorption by environmentally friendly task-specific deep eutectic solvents of PPZBr+ Gly. *ACS Sustainable Chem. Eng.* **2019**, *7*, 14236−14246.
(42) Wang, J.; Zeng, S.; Bai, L.; Gao, H.; Zhang, X.; Zhang, S. Novel ether-functionalized pyridinium chloride ionic liquids for efficient SO_2 capture. *Ind. Eng. Chem. Res.* **2014**, *53*, 16832−16839.
(43) Long, G.; Yang, C.; Yang, X.; Zhao, T.; Liu, F.; Cao, J. Bisazole-Based Deep Eutectic Solvents for Efficient SO_2 Absorption and Conversion without Any Additives. *ACS Sustainable Chem. Eng.* **2020**, *8*, 2608−2613.
(44) Sheng, K.; Kang, Y.; Li, J.; Xu, H.; Li, D. High-efficiency absorption of SO_2 by a new type of deep eutectic solvents. *Energy Fuels* **2020**, *34*, 3440−3448.
(45) Zhang, J.; Yu, L.; Gong, R.; Li, M.; Ren, H.; Duan, E. Role of Hydrophilic Ammonium-Based Deep Eutectic Solvents in SO_2 Absorption. *Energy Fuels* **2020**, *34*, 74−81.

https://doi.org/10.1021/acsomega.2c03221
ACS Omega 2022, 7, 29171−29180